Catalysis Science & Technology

PAPER

Check for updates

Cite this: *Catal. Sci. Technol.*, 2019, **9**, 6166

Fast and deep oxidative desulfurization of dibenzothiophene with catalysts of MoO_3–TiO_2@MCM-22 featuring adjustable Lewis and Brønsted acid sites†

Qian Luo,‡[a] Qi Zhou,‡[a] Yan Lin,[a] Shaohua Wu,[a] Hongyu Liu,*[a] Cheng Du,[b] Yuanyuan Zhong[b] and Chunping Yang *[ab]

Received 19th July 2019,
Accepted 28th September 2019

DOI: 10.1039/c9cy01438a

rsc.li/catalysis

The synthesis of high-performance and recyclable catalysts for oxidative desulfurization (ODS) from fuels has been a significant challenge. In this study, novel catalysts of MoO_3–TiO_2@MCM-22 with excellent catalytic performance were successfully prepared *via* a facile impregnation method. The results showed that the optimal catalyst at the Mo–Ti mass ratio of 1 : 4 (MT-1 : 4) exhibited highest catalytic efficiency for the ODS of dibenzothiophene (DBT) with a sulfur conversion of 99.96% within 15 min. Interestingly, the enhanced ODS activity was attributed to the synergistic effect between MoO_3 and TiO_2, which was achieved by adjusting the concentrations of Lewis and Brønsted acid sites on the surface of MCM-22. The catalyst MT-1 : 4 achieved the highest concentrations of Lewis and Brønsted acid sites and the largest combined index, resulting in the formation of peroxometallate complexes. Moreover, the kinetic studies revealed that the ODS was a pseudo first-order reaction with an apparent activation energy of 48.9 kJ mol^{-1}. There was no significant reduction in the catalytic activity after 8 successive cycles, which manifested the perfect reusability of the catalyst MT-1 : 4 for the ODS system. Furthermore, a plausible ODS mechanism was proposed using the MoO_3–TiO_2@MCM-22 catalyst. Therefore, the prepared MoO_3–TiO_2@MCM-22 catalyst exhibited favorable industrial application potential for ODS.

1. Introduction

In recent decades, the emission of organic sulfur compounds present in petroleum has seriously affected the air quality and further harmed human health. The sulfur content of 15 mg L^{-1} is required according to the EPA's Clean Air Highway Diesel fuel final rule; thus, engine manufacturers need to adopt advanced emission control devices to decrease harmful emissions.[1] To address the challenge, new technologies for producing ultra-low sulfur diesel have been developed in recent years. Hydrodesulfurization (HDS) is the most traditional desulfurization method for organic sulfide removal from fuel. However, HDS is carried out at high temperatures and pressures with hydrogen consumption, which significantly increases the cost of desulfurization.[2] Moreover, the desulfurization efficiency is low for the treatment of refractory benzothiophenes.[3,4] Thus, for the desulfurization of dibenzothiophene (DBT), it is of great significance to develop alternative or supplemental high-efficiency desulfurization systems.[5]

Oxidative desulfurization (ODS) is considered as a promising technology for highly efficient desulfurization owing to its mild operation conditions as well as high efficiency. Generally, ODS mainly includes two steps: an appropriate oxidizing agent oxidizes the organic sulfur compounds to sulfoxides and sulfones, and then, the oxidation products are removed by suitable methods.[6] Hydrogen peroxide (H_2O_2) has been adopted most frequently because of its good properties and low price as an oxidant.[7] Unfortunately, a biphasic system is formed due to the poor solubility of H_2O_2, which limits the mass transfer and the oxidative reactions rates are consequently suppressed.[8] To solve these problems, the use of cyclohexanone peroxide (CYHPO) as an oil-soluble oxidant was proposed for ODS.[9–12] In addition, the application of solvent extraction using acetonitrile,[3,13] [Bmim]BF_4,[14,15] methanol[16] and *N*,*N*-dimethylformamide[10] was investigated for the better removal of oxidation products (sulfone and sulfoxide)

[a] *College of Environmental Science and Engineering, Hunan University and Key Laboratory of Environmental Biology and Pollution Control (Hunan University), Ministry of Education, Changsha, Hunan 410082, China.*
E-mail: hyliu@hnu.edu.cn, yangc@hnu.edu.cn
[b] *Guangdong Provincial Key Laboratory of Petrochemical Pollution Processes and Control, School of Environmental Science and Engineering, Guangdong University of Petrochemical Technology, Maoming, Guangdong 525000, China*

† Electronic supplementary information (ESI) available. See DOI: 10.1039/c9cy01438a

‡ These authors contributed to this article equally.

This journal is © The Royal Society of Chemistry 2019

from the ODS systems. Kang *et al.* reported the removal of oxidation products by filtration, which showed the potential of being a simple, low-cost, and effective method.[17]

Catalysts are essential and important in ODS, and a lot of catalysts were investigated and reported for better catalytic performance, for example, metal organic framework (MOF)-supported catalysts[6,18] metal-based ionic liquid-supported catalysts,[14,19] metal oxides,[20–23] and Ti-containing catalysts such as Ti-SBA-15,[24] Mo/Ti-PILC,[17] Ti-SBA-16,[25] Ti-MWW,[26] and Ti-MCM-41.[27] Among them, the catalysts using molecular sieves as support and using transition metal Mo, W, Ti, Ni, Co, *etc.*, as active centers were widely used for ODS.[17] The MWW-type zeolite is a type of layered MCM-22 zeolite and possesses two coexisting pore systems, which have a wide catalytic application in the petrochemical and refining industries.[28] It was proved that the MCM-22 zeolite is a superb cracking zeolite additive in the FCC process owing to its lamellar structure, large specific surface area, and high stability.[28] However, according to existing literatures, the application of MCM-22 zeolite in ODS has not been reported.

In addition to catalyst supports, the active center is more important in some aspects. MoO_3 and TiO_2 were widely used as the active centers in ODS of DBT. For instance, Mo-containing catalysts were reported to be exceedingly successful for ODS.[29,30] Qiu *et al.*[29] exhibited that the Mo/MMS catalyst was highly efficient for the conversion of DBT from fuel. The Mo-containing system showed around 95% high selectivity towards diphenyl sulfone and nearly 90% conversion of diphenyl sulfide.[31] Furthermore, BAS and LAS were two types of acidic species on the surface of the catalyst. BAS was a kind of substance that can give protons according to the proton theory proposed by Brønsted and Lowry. LAS is a kind of substance that can accept electron pairs according to the electronic theory proposed by Lewis.[32,33] Numerous reports drew the conclusion that the catalyst acidity (Lewis and Brønsted acid sites) was the key for the enhancement of efficiency in ODS processes. Muñoz *et al.*[31] indicated that the increase in Lewis acid sites concentration could be due to the presence of Mo in the ODS system, which demonstrated that the Lewis acid sites played a vital role in ODS.

Recently, titania (TiO_2) has not only been used as a modifier for the support of catalysts but also as an active center for the high-efficiency ODS of organic sulfur compounds. TiO_2 is a very appealing material for ODS of DBT due to the unique physical and chemical characteristics, earth abundance, non-toxicity, as well as the high thermal and chemical stability.[34] TiO_2 was generally found in four crystal forms: tetragonal anatase, tetragonal rutile, monoclinic TiO_2(B), and orthorhombic brookite.[35] Amin Bazyari *et al.*[36] suggested that anatase was believed to perform better than other crystalline polymorphs with respect to the catalytic activity. Meanwhile, the presence of anatase TiO_2 was related to the Brønsted acid sites, which were generated while TiO_2 and SiO_2 formed the Ti–O–Si chemical bonds.[37] Importantly, it was demonstrated that there was a direct relationship between the catalytic ODS efficiency and the density of Brønsted acid sites, and the different distribution of Lewis and Brønsted acid sites could enhance the catalytic activity of the catalysts.[38]

Therefore, MoO_3 and TiO_2 were used as the active centers in the catalysts, which had the potential for improving the performance of ODS, such as the enhancement of the removal rates and the shortening of reaction time. It could be deduced that there existed synergistic effects between MoO_3 and TiO_2, which improved the desulfurization rate. However, up to now, there has been no report using MoO_3 and TiO_2 simultaneously as active centers to achieve fast and deep desulfurization.

In this work, novel catalysts of MoO_3–TiO_2@MCM-22 were synthesized by a facile method for the first time, in which MoO_3 and TiO_2 simultaneously acted as the active centers. The micro-morphological structures, chemical compositions, and catalytic activities of the as-prepared catalysts were fully characterized and discussed. The catalytic performance on ODS of DBT with the oil-soluble oxidant of CYHPO was discussed in detail. Moreover, the effects of different Mo–Ti mass ratios, reaction conditions and calcination temperatures on the ODS performance were investigated for the optimization of desulfurization conditions, and subsequently the kinetics and possible mechanism of ODS were studied. This material exhibited superior application value with fast and deep oxidative desulfurization in the industry.

2. Experimental

2.1. Chemicals

Aluminosilicate MWW (MCM-22, SiO_2/Al_2O_3 = 25) was obtained from Yuanli Chemical Co. Ltd. (Tianjin, China). Cyclohexanone peroxide (CYHPO, 50%) and dibenzothiophene (DBT, 98%) were obtained from Aladdin Reagent Co. Ltd. (Shanghai, China). Tetrabutyl titanate ($Ti(C_4H_9O)_4$), ammonium hepta molybdate ($(NH_4)_6Mo_7O_{24}{\cdot}4H_2O$), and absolute ethanol (CH_3CH_2OH) were obtained from Sinopharm Chemical Reagent Co., Ltd (Shanghai, China). *N*-Octane (C_8H_{18}, 96%) was produced from Kemiou Chemical Reagent Co. Ltd. (Tianjin, China). All the reagents used were of analytical grade. Ultra-pure water (18.2 MΩ cm) was used in the experiments.

2.2. Preparation of catalysts

The preparation of H-MCM-22 was based on the modified method of Wang *et al.*[28] In brief, 1.0 g MCM-22 was placed in a 100 mL beaker with 50 mL 1 M NH_4NO_3 and the mixed solution was stirred for 2 h at 353 K. After that, the light yellow precipitate was collected by centrifugation, washed by ultrapure water three times, and dried in vacuum (333 K) overnight. For sufficient ammoniation, the obtained light yellow solids were placed in a 100 mL beaker with 50 mL 1 M NH_4NO_3 again and then the above procedures were repeated. Then, the light yellow solids were placed in a crucible and calcined at a rate of 5 K min^{-1} at 823 K for 3 h in a muffle furnace. Finally, the white products (H-MCM-22) were obtained and then milled for 20 min at room temperature.

MoO_3–TiO_2@MCM-22 catalysts were synthesized by a facile impregnation method together with ultrasonic-assisted dispersion. Firstly, 0.500 g of H-MCM-22 was dispersed into ultra-pure water (50 mL) *via* sonication for 0.5 h (solution A). Secondly, 0.0920 g $(NH_4)_6Mo_7O_{24}{\cdot}4H_2O$ was added in 5 mL ultra-pure water (solution B) and 1.42 mL $Ti(C_4H_9O)_4$ was added in 5 mL of absolute ethanol (solution C). The solutions B and C were simultaneously added dropwise to solution A, and the mixed solution was stirred under room temperature for 4 h. After that, the mixed solution was impregnated for 24 h. The precipitates were obtained by centrifugation, washed with ultra-pure water several times, and dried in vacuum (333 K) overnight. Finally, the above dried catalysts were heated at 823 K for 3 h by using a muffle furnace. MoO_3–TiO_2@MCM-22 with the Mo–Ti mass ratio of 1 : 4 was denoted as MT-1 : 4. Likely, other MoO_3–TiO_2@MCM-22 samples were denoted as MT-0 : 5, MT-2 : 3, MT-1 : 1, MT-3 : 2, MT-4 : 1, and MT-5 : 0 based on the various mass ratios of Mo and Ti on MCM-22.

2.3. Characterization

N_2 adsorption–desorption isotherms (Micromeritics Tristar II 3020 apparatus) were used to record the textural properties of the materials. The microstructures and morphologies of the catalysts were determined with a high resolution transmission electron microscope (HRTEM, TecnaiG2 F20, FEI) and a scanning electron microscope (SEM, JEOL JSM-6700). The crystal structures of the materials were measured by X-ray diffraction (XRD) with a Rigaku Dmax 2500 diffractometer equipped with monochromatic Cu Kα radiation. Fourier transform infrared spectroscopy (FTIR) was performed on a VARIAN 3100 spectrometer using the potassium bromide (KBr) pellet technique for obtaining chemical bonding information of the materials. X-ray photoelectron spectroscopy (XPS, Thermo Fisher) was performed to record the chemical compositions of the materials. The acidity of the prepared catalysts was measured by temperature-programmed desorption of ammonia (NH_3-TPD) performed on a Micromeritics AutoChem II 2920 apparatus using a TCD detector with NH_3/He flow. The acidic properties of the materials were detected by the FTIR spectra of adsorbed pyridine (pyridine-adsorption FTIR), using a PE Frontier FT-IR Spectrometer (the detailed procedures are presented in the ESI†). The amount of molybdenum and titanium in MoO_3–TiO_2@MCM-22 was determined by inductively coupled plasma OES spectrometer (ICP-OES) using an Ultima2 HORIBA Jobin Yvon spectrometer.

2.4. ODS reaction and separation of oxidation products

In a typical experiment, ODS reactions of the prepared samples towards DBT were carried out in the Erlenmeyer flasks (50 mL) with a magnetic stirrer. The reaction procedure was as follows: 20 mL of model oil with a sulfur content of 500 mg L^{-1}, 0.05–0.20 g catalysts, and a certain amount of CYHPO (O/S = 1.0, 1.5, 2.0, and 2.5) were added into the Erlenmeyer flasks. After that the Erlenmeyer flasks were placed in the oil bath pan to react for 30 min at 313, 333, 353, 373, and 393 K, respectively. All the samples were withdrawn at the predetermined times of 5, 10, 15, 20, 25, and 30 min, and then the Erlenmeyer flasks were cooled down for half an hour at room temperature. The solid catalysts were filtered out of the oxidized oil and the sulfur-containing oxidation products were separated from the oxidized oil by a 0.45 μm organic filter membrane. The sulfur concentration was measured by a gas chromatograph (GC; Agilent-7890N; FID, HP7890) using a HP-5 capillary column (30 m long × 0.25 mm I.D. × 10.25 μm film thickness).

2.5. Regeneration of the catalysts

To study the regeneration of the catalysts, the spent samples were regenerated by a high temperature calcination method after the oxidation reactions. The spent samples were calcined at 823 K for 3 h by using a muffle furnace. The regenerated catalysts were collected and then used in new reaction runs.

3. Results and discussion

3.1. Characterization of the samples

The microstructures and morphologies of the catalysts were determined by SEM (Fig. 1(A–C)). It could be clearly seen that MCM-22 was made up of thin flake-like crystals, especially in Fig. 1C, which was consistent with the findings of Wang *et al.*[39] It was observed that a large number of MoO_3 and TiO_2 particles were distributed unevenly on the intergrown flaky crystals of the MCM-22 molecular sieve in Fig. 1A and C, respectively, which were the results of the agglomerations of TiO_2 and MoO_3 during crystallization. Interestingly, under the same scope of the SEM image (Fig. 1B, 2 μm), a few MoO_3 and TiO_2 particles were homogeneously distributed on the surface of MCM-22. It was concluded that the coexistence of TiO_2 and MoO_3 dispersed their active centers well on the support.

In order to further illustrate the above results and gain the detailed structural information, MT-1 : 4 was characterized by transmission electron microscopy (TEM) image and the result is presented in Fig. 1D and S1.† The interplanar distance of 0.352 nm corresponded well to the (101) plane of the anatase TiO_2 (JCPDS card No. 21-1272) and the (101) crystal plane of anatase TiO_2 was reported in the study of Yue *et al.*[40] Moreover, the interplanar spacing of 0.345 nm was obtained, which corresponded to the (210) crystallographic planes of MoO_3 (JCPDS card No. 21-0569). Besides, as displayed in Fig. S1,† the average particle sizes of TiO_2 and MoO_3 were 3.49 nm (1.50–6.50 nm) and 6.92 nm (3.00–13.00 nm), respectively. The average pore size of MCM-22 was 6.71 nm (Table 1), which indicated that small-sized MoO_3 and TiO_2 particles could be introduced into the pores of MCM-22; the large-sized MoO_3 and TiO_2 particles were supported on the surface of MCM-22. It can be rationally concluded that MoO_3 and TiO_2 were successfully supported on MCM-22.

MCM-22, MT-0 : 5, MT-1 : 4, and MT-5 : 0 were determined by nitrogen adsorption measurements to obtain the textural properties of the samples. The textural parameters were

 This journal is © The Royal Society of Chemistry 2019

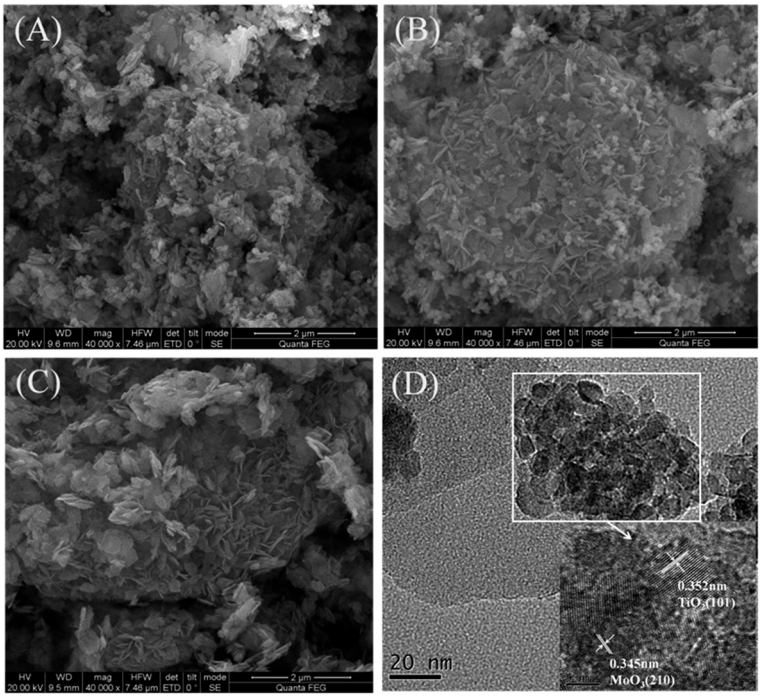

Fig. 1 SEM images of (A) MT-0 : 5; (B) MT-1 : 4; (C) MT-5 : 0. HRTEM image of (D) MT-1 : 4.

presented in Table 1; the nitrogen adsorption–desorption isotherms and pore size distributions of the samples are presented in Fig. 2. The N_2 adsorption–desorption isotherms for the as-prepared catalysts showed type II isotherms typically with a type H3 hysteresis, indicating the presence of a mesoporous structure with the micropores on the basis of the studies[41–43] (Fig. 2A). Based on the classification of the pores (IUPAC), the pore size under 2 nm is called a micropore and the pore size of a mesopore ranges from 2 to 50 nm. As presented in Fig. 2(B–E), the results of the pore size distribution were in agreement with the N_2 adsorption–desorption isotherms. The microporous area (S_{Micro}) of MCM-22, MT-5 : 0, MT-1 : 4, and MT-0 : 5 were 445, 429, 207, and 194 $m^2\ g^{-1}$, respectively, which demonstrated that most of the MoO_3 and TiO_2 particles were introduced into the pores of MCM-22. This was consistent with the change in the pore volume (Table 1). In addition, the results of the external surface areas (S_{Ext}) manifested that a small part of MoO_3 and TiO_2 particles were supported on the surface of the MCM-22. The specific surface areas (S_{BET}) of MT-0 : 5 and MT-1 : 4 were respectively 312 and 327 $m^2\ g^{-1}$, which had no significant difference. However, the S_{BET} of MT-5 : 0 was 534 $m^2\ g^{-1}$, which was almost twice that of MT-0 : 5 and MT-1 : 4. In addition, the pore volume of MT-5 : 0 was nearly twice that of MT-0 : 5 and MT-1 : 4, which was consistent with the change in S_{BET}. It was due to the fact that the TiO_2 particles blocked the pores of MCM-22, resulting in the concomitant reduction of S_{BET} and pore volume. Additionally, the decrease in S_{BET} could be partly attributed to an increase in the mass of Ti atoms or an enhanced contribution of the pure TiO_2 properties.[36] Based on the above results, it was summarized that the as-prepared catalysts revealed the presence of the mesoporous structure with the micropores possessing a large S_{BET}, which endowed the catalysts with sufficient active sites for ODS.

X-ray diffraction (XRD) was employed to record the crystal structure properties of the catalysts and the patterns are shown in Fig. 3. The diffraction peaks at 2θ = 25.28°, 37.80°, 48.05°, 53.89°, 55.06°, and 62.69° could be indexed to the (101), (004), (200), (105), (211), and (204) planes, respectively, which corresponded to the anatase phase TiO_2 (PDF No. 21-1272). In addition, except for the (101) reflection peaks, other peaks of anatase TiO_2 gradually disappeared from MT-1 : 1 to MT-4 : 1 in Fig. 3. It was attributed to the fact that TiO_2 exhibits dispersed and highly crystalline phases or disordered/amorphous phases on the catalyst surfaces when TiO_2 content was low, which caused that these peaks could not be observed.[44,45] This result was also consistent with the ICP results, which displayed that the content of Mo and Ti was 4.50% and 18.2% in MT-1 : 4, respectively. The peak of MT-5 : 0 at 25.80° could be indexed to the (210) plane from the characteristic diffraction peaks of MoO_3 (PDF No. 21-0569). No peak attributed to MoO_3 was observed in the XRD pattern of MT-1 : 1. On the basis of the monolayer dispersion theory,[46] it may be due to the fact that most of the TiO_2 on the catalyst was amorphously dispersed on MCM-22 (SiO_2/Al_2O_3 = 25) when the Mo/Ti mass ratio was 1 : 1, which promoted the high dispersion of MoO_3 on MCM-22, thus eventually resulting in no peak of MoO_3 in the XRD pattern of the catalyst MT-1 : 1. The peaks of the catalysts with different Mo–Ti mass ratios were identical to that of pure TiO_2 and pure MoO_3 without any shift. The findings of XRD were in accordance with the SEM

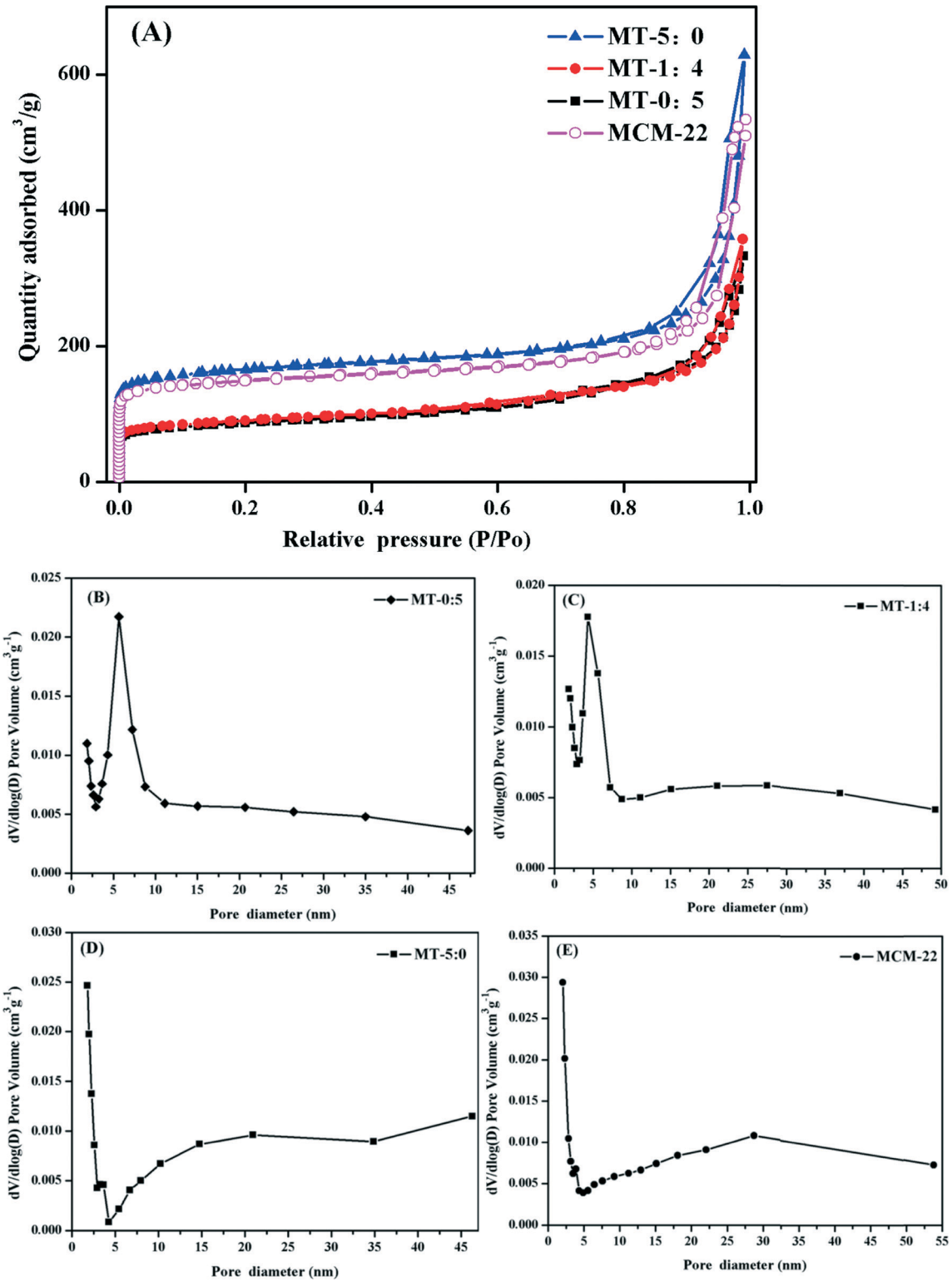

Fig. 2 (A) N_2 adsorption–desorption isotherm of the as-prepared samples; (B, C, D and E) pore size distribution of MT-0 : 5, MT-1 : 4, MT-5 : 0 and MCM-22, respectively.

results, which further substantiated that MoO_3 and TiO_2 were successfully supported on the MCM-22.

The FT-IR spectra of MT-0 : 5, MT-1 : 4, and MT-5 : 0 were obtained to explore the bonding composition and functional groups of the catalysts (Fig. 4). All the spectra displayed the absorption peaks at 3430 and 1636 cm^{-1}, which corresponded to O–H stretching vibration of adsorbed water between the MCM-22 layers.[28] According to the literature,[24,47] the peaks at

 This journal is © The Royal Society of Chemistry 2019

Table 1 Physical properties of catalytic materials used in the ODS experiments

Sample	S_{BET}[a] ($m^2\ g^{-1}$)	S_{Ext}[b] ($m^2\ g^{-1}$)	S_{Micro}[b] ($m^2\ g^{-1}$)	Pore volume[c] ($cm^3\ g^{-1}$)	Average[d] pore size (nm)
MT-0 : 5	312	118	194	0.51	6.40
MT-1 : 4	327	120	207	0.55	6.58
MT-5 : 0	534	105	429	0.97	6.12
MCM-22	593	148	445	1.21	6.71

[a] Measured using N_2 adsorption with the Brunauer–Emmett–Teller (BET) method. [b] Calculated by the *t*-plot method and the Barrett–Joyner–Halenda (BJH) method, respectively. [c] Single point adsorption total pore volume of the pores determined at P/P_0 = 0.99. [d] Calculated by the *t*-plot method and the Barrett–Joyner–Halenda (BJH) method, respectively.

1095 and 451 cm^{-1} corresponded to the asymmetric stretching vibrations of the Ti–O–Si bonds of the MCM-22 framework. Moreover, the FT-IR spectrum of MT-5 : 0 exhibited a peak at 811 cm^{-1}, which corresponded to the asymmetrical stretching vibration of the Mo–O bond of MoO_3.[48] The FT-IR peak at 605 cm^{-1} was characteristic of octahedral aluminum, according to the report by Sidra Subhan *et al.*[1] In addition, the peaks ranging from 500 to 900 cm^{-1} and 400–900 cm^{-1} were assigned to Al–O (ref. 49) and the bending vibration absorption peak of the Ti–O,[50] respectively. Accordingly, the peak at 560 cm^{-1} was ascribed to the Ti–O and Al–O bonds. The FT-IR results proved that the catalysts MoO_3–TiO_2@MCM-22 were successfully prepared.

X-ray photoelectron spectroscopy (XPS) was adopted to examine the elemental chemical compositions and chemical status of MT-1 : 4. As shown in Fig. 5A, all elements such as Mo, Ti, O, Al, and Si could be observed in the XPS survey spectrum. Two peaks of the Mo^{6+} species (MoO_3) were found at 236.40 and 233.20 eV, which were put down to the Mo $3d_{3/2}$ and Mo $3d_{5/2}$ states (MT-1 : 4 of Fig. 5(B)),[48] respectively. The peak for Ti $2p_{1/2}$ could be observed at 464.80 eV and Ti $2p_{3/2}$ was located at 459.00 eV (MT-1 : 4 of Fig. 5(C)), which indicated the chemical valence state of Ti^{4+}.[35] It was proved that Mo^{6+} and Ti^{4+} were formed in MT-1 : 4, which was in agreement with the findings of XRD. Besides, it was found that the peaks of Ti $2p_{1/2}$ and Ti $2p_{3/2}$ were located at 465.00 and 459.30 eV, respectively, which could be ascribed to Ti^{4+} in TiO_2 (Fig. S2(A)†). The spectrum in Fig. S2(B)† indicated that the small peak of Mo $3d_{5/2}$ was located at 233.40 eV, which was due to the amorphous phase of MoO_3 on the surface of MCM-22.[3] In the range of Mo/Ti mass ratio from 1 : 4 to 4 : 1, the binding energies of Mo 3d and Ti 2p both moved towards a high level, which may be due to the electron donor effect of Mo and Ti. However, compared with that of pure Ti (MT-0 : 5) and pure Mo (MT-5 : 0) catalysts, the other Mo/Ti ratio of the catalysts shifted slightly to low or high binding energies, indicating that Mo and Ti may regulate the acidity of the catalysts by gaining electrons or acting as electron donors.[3,51] Notably, compared with the XPS profiles of MT-0 : 5 and MT-5 : 0, the binding energies of Mo and Ti in MT-1 : 4 both shifted slightly to a low level. In addition, the binding energy was negatively related to the surface electron density.[52] Therefore, the results indicated that the electron transfer occurred from MCM-22 to Mo and Ti in MT-1 : 4. The XPS findings further proved the successful combination of MoO_3 and TiO_2 in the MoO_3–TiO_2@MCM-22 catalyst.

To ascertain the amount and properties of Lewis and Brønsted acid sites on the catalysts, Py-FTIR was measured and the results are presented in Fig. 6 and Table 2. As shown in Fig. 6, the vibrations at 1630 and 1450 cm^{-1} were assigned to pyridine adsorbed on Lewis acid sites (LAS) and the intensity of the band at 1630 cm^{-1} gradually increased due to the

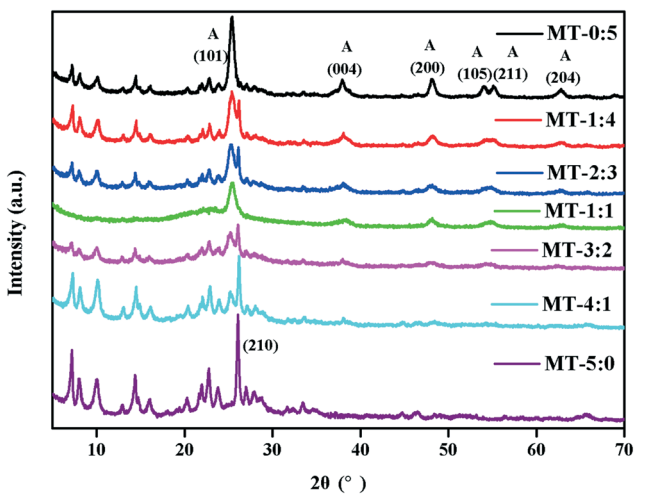

Fig. 3 XRD pattern of the as-prepared samples.

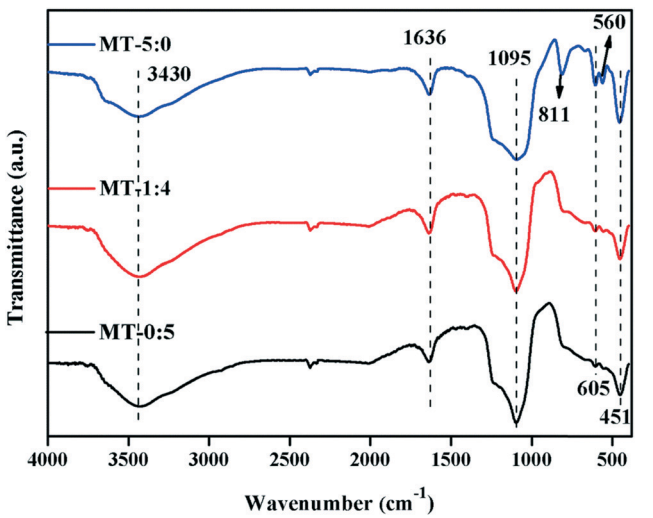

Fig. 4 FTIR patterns of the MT-0 : 5, MT-1 : 4 and MT-5 : 0 catalysts.

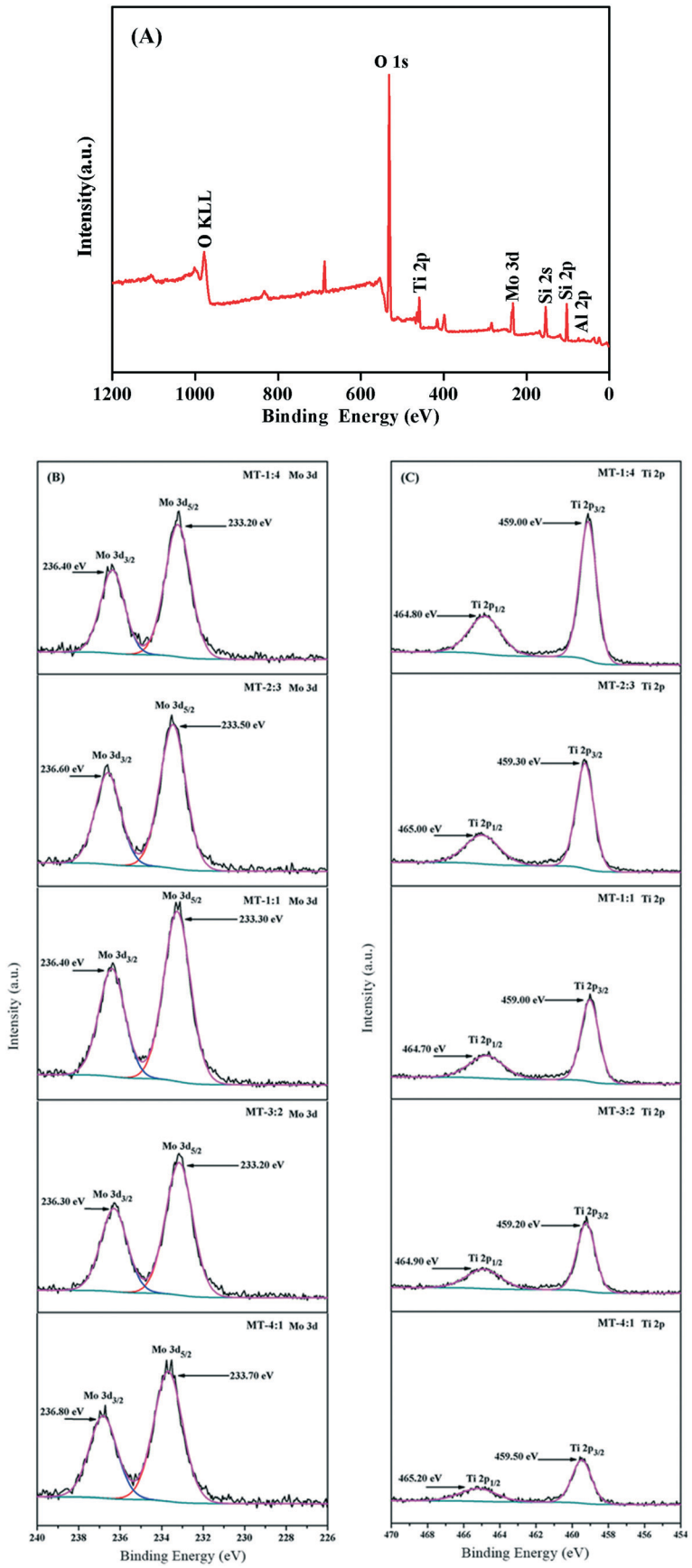

Fig. 5 (A) XPS survey spectra and (B) and (C) high-resolution XPS spectrum of Mo 3d and Ti 2p, respectively.

This journal is © The Royal Society of Chemistry 2019

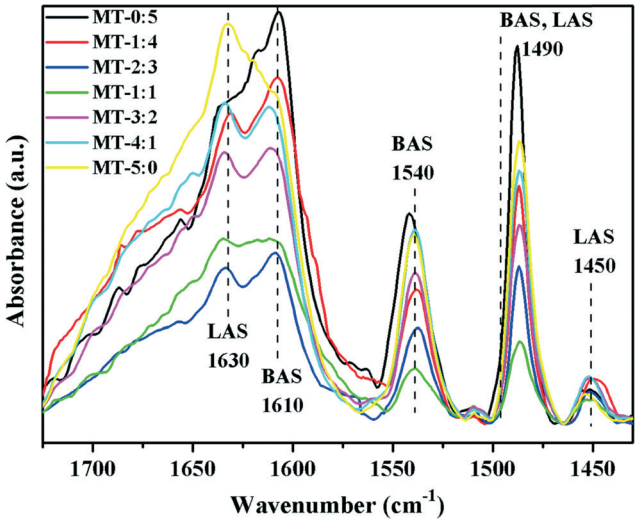

Fig. 6 FTIR spectra of pyridine absorbed at 623 K on the as-prepared catalysts.

Mo species.[31] Besides, the intensity of the peak at 1610 cm^{-1} corresponded to the Brønsted acid sites (BAS) owing to Ti species on the support.[53,54] The band at 1540 cm^{-1} corresponded to pyridine adsorbed on BAS and the vibration at 1490 cm^{-1} was assigned to pyridine adsorbed on both LAS and BAS.[32] BAS were generated when TiO_2 and SiO_2 formed Ti–O–Si chemical bonds.[37] Moreover, Brønsted acidity was created when the hydroxyl groups balance the charge imbalance, which occurred in the Ti–O–Si bonds as the tetrahedral Si atoms were isomorphously substituted for Ti atoms.[53] However, LAS were generated by metal-O groups and the increase in LAS concentration could be due to the presence of Mo in the ODS system, according to the study of Muñoz *et al.*[31] In addition, Rodriguez-Gattorno *et al.*[38] suggested that the coexistence of Lewis and Brønsted acid sites vigorously promoted the formation of peroxometallate complexes, and the sulfur conversion could reach a maximum when the Brønsted acidity reached a maximum and Lewis acidity tended to a minimum. Interestingly, it was obvious that the optimal mass ratio of Mo and Ti in the catalyst was 1 : 4 for the highest catalytic efficiency in this work. Thus, there was a direct relationship between the catalytic ODS efficiency and the concentrations of LAS and BAS. It was important to keep a balance between LAS and BAS to obtain high sulfur conversion, which explained the highest catalytic activity of MT-1 : 4. As seen in Fig. 6, the intensity of the peaks of LAS and BAS varied with the Mo–Ti mass ratios. It was demonstrated that Mo and Ti were related to LAS and BAS, respectively.

Table 2 Acidic properties of the as-synthesized catalysts

Catalyst	Lewis[a] (mmol g^{-1})	Brønsted[a] (mmol g^{-1})	Combined index	Total acidity[b] (mmol g^{-1})
MT-0 : 5	0.005	0.112	—	0.534
MT-1 : 4	0.017	0.079	2.59	1.160
MT-2 : 3	0.010	0.051	1.57	0.593
MT-1 : 1	0.007	0.026	1.01	0.569
MT-3 : 2	0.014	0.075	2.23	0.663
MT-4 : 1	0.015	0.074	2.33	0.790
MT-5 : 0	0.009	0.092	—	0.446

[a] Determined by Py-FTIR and NH_3-TPD, respectively. [b] Determined by Py-FTIR and NH_3-TPD, respectively.

In addition, the concentrations of the LAS and BAS were obtained *via* eqn (1) and (2), respectively,[32] and are presented in Table 2.

$$C_L(\mu molg^{-1}) = \frac{1.42 \times IA_L \times R^2}{W} \quad (1)$$

$$C_B(\mu molg^{-1}) = \frac{1.88 \times IA_B \times R^2}{W} \quad (2)$$

where C_L and C_B were the concentration of LAS and BAS, respectively, IA_L and IA_B were the integrated absorbance bands for LAS and BAS, respectively, R was the radius of the catalyst disk and W was the weight of the disk.

Besides, it was assumed that Mo and Ti regulated the amounts of LAS and BAS, respectively. The combined index[55] of the catalysts may be expressed as

$$CI = \frac{C_L}{C_{LX}} + \frac{C_B}{C_{BX}} \quad (3)$$

where, CI was the combined index of the catalysts, and C_L and C_B stood for the concentration of LAS and BAS in the catalyst under the synergy of Mo and Ti, respectively. C_{LX} and C_{BX} represented the concentration of LAS and BAS in the catalyst under pure Mo or pure Ti, respectively.

As seen from Table 2, Mo and Ti adjusted the concentrations of LAS and BAS. Catalyst MT-1 : 4 had the highest concentrations of LAS and BAS, and the CI value was also the largest. Thus, it could be concluded that MT-1 : 4 showed the best synergistic effect of Mo and Ti by adjusting LAS and BAS, which was consistent with the highest catalytic efficiency of ODS with the catalyst MT-1 : 4. In order to further confirm the aforementioned results, the acidity of the prepared catalysts was measured by NH_3-TPD. The area under the NH_3-TPD profile represented the amount of acid sites.[28,36] The results are displayed in Fig. S3† and Table 2. There were two desorption peaks called h-peak and l-peak in all these profiles, where the h-peak could be assigned to the desorption of NH_3 from the strong Brønsted and Lewis acid sites, which were of catalytic importance.[28] The results of NH_3-TPD were essentially consistent with the results of Py-FTIR. On the basis of the above results, the following experiments were performed to further confirm the best performance of the MT-1 : 4 catalyst.

3.2. Effects of mass ratios of Mo and Ti on ODS

The catalysts of different Mo–Ti mass ratios had different species of active sites, which could regulate the distribution of acidity on the catalyst surface and further affected the synergistic effect, so that the catalysts could attain the highest efficiency on oxidative desulfurization of DBT. In order to investigate the effects of different mass ratios of Mo and Ti on

catalytic ODS, seven samples with different mass ratios of Mo and Ti were prepared: MT-0 : 5, MT-1 : 4, MT-2 : 3, MT-1 : 1, MT-3 : 2, MT-4 : 1, and MT-5 : 0. The performance of these samples was obtained for oxidative reactions of the model oil at 373 K for 30 min (Fig. 7A).

The sulfur conversion rate was defined as the concentration of sulfur converted from the model oil with respect to the initial concentration of sulfur (multiplied by 100). As presented in Fig. 7A, the sulfur conversion rates increased and then gradually plateaued with increasing time, indicating that all the prepared catalysts had catalytic capability in ODS of DBT. After 30 min of reaction, the sulfur conversion rates for the catalysts supported with Mo and Ti (MT-4 : 1, MT-3 : 2, MT-1 : 1, MT-2 : 3, and MT-1 : 4) reached 99.96%, while the sulfur conversion rates of the catalysts with pure Mo (MT-5 : 0) and pure Ti (MT-0 : 5) were only 54.31% and 67.43%, respectively. It indicated that the catalysts simultaneously supported with Mo and Ti were superior to pure Mo and Ti for ODS of DBT. Thus, Mo and Ti on MCM-22 had synergistic effect for oxidative desulfurization. Bazyari *et al.*[36] reported

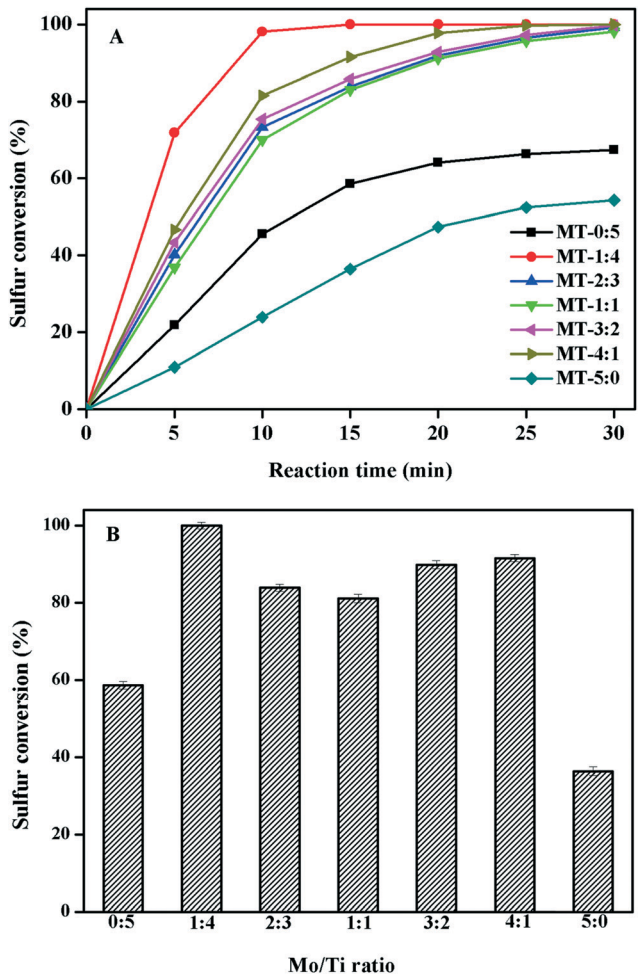

Fig. 7 Dependence of sulfur conversion *vs.* reaction time on the mass ratio of different molybdenum–titanium catalysts (A) and the comparison of ODS activities after 15 min of reaction (B). Reaction conditions: 20 mL of model fuel, 373 K, 0.10 g catalyst and O/S = 2.0.

that Ti species were the key components and Kang *et al.*[17] deemed Mo as the best active substance for oxidative desulfurization. So, it was possible that the combination of the unique properties of Mo and Ti could further exert superior activity of the catalysts and thus enhanced the performance of oxidative desulfurization. Besides, among the catalysts supported with Mo and Ti (MT-4 : 1, MT-3 : 2, MT-1 : 1, MT-2 : 3, and MT-1 : 4), MT-1 : 4 presented the highest sulfur conversion rate. For example, the sulfur conversion rate of MT-1 : 4 reached 99.96% in 15 min and the catalytic activity of MT-1 : 4 within 15 min contrasted sharply with other catalysts in Fig. 7B. The overall sulfur conversion rates were enhanced in the following order: MT-5 : 0 < MT-0 : 5 < MT-1 : 1 < MT-2 : 3 < MT-3 : 2 < MT-4 : 1 < MT-1 : 4. With the increase in Mo content, the sulfur conversion rates improved sharply at the beginning and then declined after reaching a maximum value. The conversion was not linear with the Mo/Ti ratio, which may be affected by other factors. From the results of Table 1, the S_{BET} of MT-0 : 5 and MT-5 : 0 were 312 and 534 $m^2\ g^{-1}$, respectively. This indicated that Mo and Ti have different effects on the S_{BET} of the catalyst, which resulted in a large difference in the S_{BET} of the catalysts with different Mo/Ti ratios. Thus, the amount of active sites on the catalysts and the synergistic effect between BAS and LAS were also affected. Therefore, the conversion of the catalysts was not only related to the concentrations of BAS and LAS but also related to factors such as S_{BET}.

To further investigate the catalytic activity of MT-1 : 4 in the ODS, three sets of comparative experiments were conducted on the model fuel at 373 K: (1) desulfurization using O/S = 4.0 of CYHPO without MT-1 : 4; (2) desulfurization using 0.100 g of MT-1 : 4 without CYHPO; (3) desulfurization using 0.100 g of MT-1 : 4 and O/S = 2.0 of CYHPO; the results are displayed in Table 3. The results from experiment (1) manifested that the sulfur conversion rates varied from 4.13% to 6.21% with the reaction time ranging from 15 to 30 min in the absence of MT-1 : 4. It was clearly indicated that CYHPO displayed little sulfur conversion rate without a catalyst. The experiment (2) showed that the sulfur conversion rates after 15 min and 30 min of the reaction time were respectively 3.22% and 2.58%, in the absence of the oxidant (CYHPO), indicating that the MT-1 : 4 exhibited an extremely low and unstable adsorption capacity for DBT. Compared with the results from experiments (1) and (2), experiment (3) presented that the sulfur conversion rate was 99.96% in the presence of CYHPO and MT-1 : 4 after 15 min, showing that MT-1 : 4 acted as a catalyst rather than as an adsorbent in the ODS process. It was worth noticing that experiment (1) was conducted at an O/S molar ratio of 4.0 without the catalyst, while the O/S molar ratio was 2.0 with the catalyst in experiment (3). It was indicated that the increase in the oxidant amount could scarcely improve the sulfur conversion rates for DBT but the presence of MT-1 : 4 and CYHPO could significantly reduce the activation energy of the reaction, thereby improving the sulfur conversion rates. Thus, catalyst MT-1 : 4 played an important role in achieving the ultra-deep and

 This journal is © The Royal Society of Chemistry 2019

Table 3 Comparative experiments with/without oxidant and with/without catalyst

Entry	Catalyst and/or oxidant	Sulfur conversion (%)	
		15 min	30 min[e]
1[a,b]	CYHPO	4.13	6.21
2[a,c]	MT-1 : 4	3.22	2.58
3[a,d]	MT-1 : 4 and CYHPO	100	100

[a] Model oil: DBT (sulfur content of 500 mg L^{-1}). [b] O/S (molar ratio) = 4.0. [c] Catalyst: 0.10 g of MT-1 : 4. [d] Catalyst: 0.10 g of MT-1 : 4 and O/S = (molar ratio) = 2.0. [e] Overall reaction time: 30 min.

high-efficiency ODS for DBT. The remaining experiments were conducted on MT-1 : 4 since it exhibited the highest catalytic activity among all the catalysts in this paper.

3.3. Effects of calcination temperature on the ODS of DBT

To examine the effects of different calcination temperatures on the oxidative desulfurization performance of DBT, four calcination temperatures were studied in this experiment, which were 623, 723, 823, and 923 K. The MT-1 : 4 catalyst was calcined at various temperatures and the effects are presented in Fig. 8. It could be found that the calcination temperatures had a remarkable influence on the catalytic performance of MT-1 : 4, particularly in a short reaction time, as shown in the inset of Fig. 8. As displayed in Fig. 8, the catalytic performance increased with an increase in calcination temperature from 623 to 823 K, and then decreased at a higher calcination temperature of 923 K. The as-prepared catalysts with the calcination temperature at 823 K reached a sulfur conversion rate of 99.96% within 15 min, suggesting that appropriate calcination temperature was important for the catalytic activity of MT-1 : 4. On the basis of the study,[36] the excessive calcination temperature could result in the reduction of S_{BET} of the catalyst so that the sulfur conversion rates decreased. In addition, excessive calcination temperatures would change the crystalline polymorphs of TiO_2 from the anatase to the rutile phase, which was not advantageous as the anatase phase has better catalytic activity than the rutile phase.[34,35,56] Moreover, the XRD results showed that TiO_2 formed the anatase phase in the catalyst at a calcination temperature of 823 K. Therefore, the calcination temperature of 823 K was the most suitable temperature for MT-1 : 4.

3.4. Effects of catalyst dosage and O/S molar ratio on ODS of DBT

Studies[9,57–59] have shown that catalyst dosage and O/S molar ratio are important factors for oxidative desulfurization. For better understanding the effects of different catalyst dosages and O/S molar ratios on the oxidative desulfurization performance of DBT, the amount of catalyst (0.05–0.20 g) and O/S molar ratio (1.0–2.5) were studied in this experiment. The results with different catalyst dosages and O/S molar ratios are presented in Fig. 9. As shown in Fig. 9, the efficiency was continuously enhanced when the catalyst dosage increased

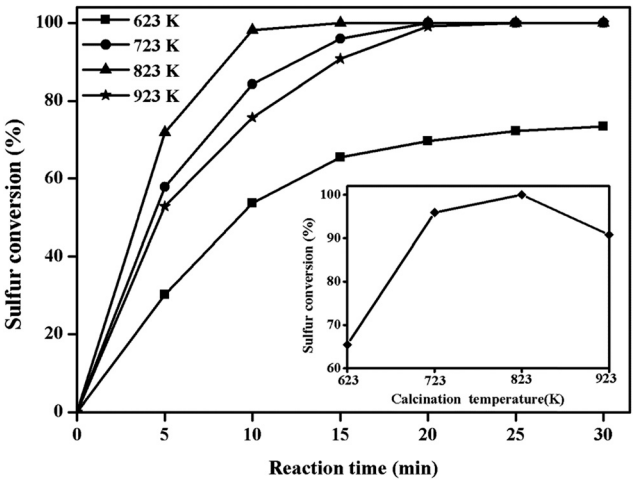

Fig. 8 Dependence of the sulfur conversion (%) *vs.* reaction time on the calcination temperature of MT-1 : 4 (inset showed the DBT removal *vs.* calcination temperature over MT-1 : 4 after 15 min of the reaction). Reaction conditions: 20 mL of model fuel, 373 K, 0.10 g catalyst and O/S molar ratio of 2.

from 0.05 to 0.10 g and then tended to be balanced from 0.10 to 0.20 g. The DBT reached a conversion rate of 99.96% with a catalyst dosage of only 0.10 g within 15 min, indicating that the increase in the catalyst dosage could improve the number of active sites, which led to the enhancement of catalytic efficiency. However, the sulfur conversion rates reached saturation as the amount of the catalyst was further increased to 0.2 g. Based on the above investigation, 0.10 g of MT-1 : 4 was selected as the optimal dosage for oxidative desulfurization. In addition, Fig. 9 exhibits the effects of O/S molar ratio on oxidative desulfurization. It was obvious that the sulfur content rapidly decreased from 176.21 to 0 mg L^{-1} within 15 min when the O/S molar ratio rose from 1.0 to 2.0. Moreover, the sulfur content reached the lowest level and the excessive oxidants did not react when O/S molar ratio was

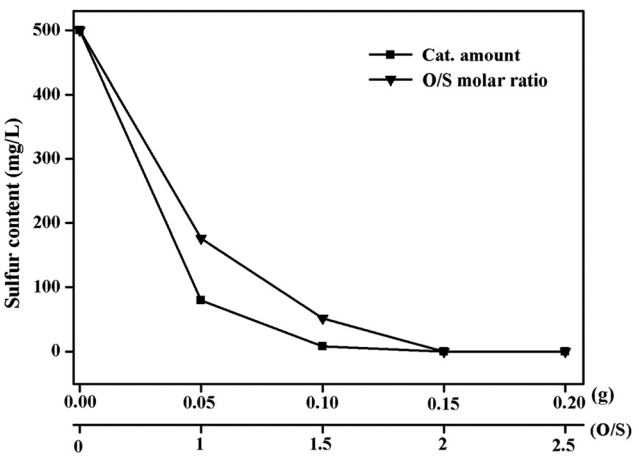

Fig. 9 Effects of amount of catalyst and O/S molar ratios on the oxidation of DBT. Amount of MT-1 : 4 catalyst (O/S = 2.0, $V_{model\ oil}$ = 20 mL, t = 15 min, and T = 273 K). Molar ratio of O/S ($M_{catalyst}$ = 0.10 g, $V_{model\ oil}$ = 20 mL, t = 15 min, and T = 273 K).

further increased to 2.5, indicating that the oxidant dosage reached saturation when the O/S molar ratio was 2.0. Thus, an O/S molar ratio of 2.0 was selected as the optimum value for sulfur conversion.

3.5. Effects of reaction temperature and kinetics of catalytic oxidation

The effects of reaction temperature on the ODS efficiency was investigated and the results from 313 to 393 K are presented in Fig. 10. With the temperature increasing from 313 to 373 K, the sulfur conversion rates were greatly promoted from 7.77% to 99.96% within 15 min and reached equilibrium. Nevertheless, the sulfur conversion rates gradually decreased to 90.33% within 15 min when the reaction temperature varied from 373 to 393 K. Based on the studies of Qiu *et al.*[29] and Yang *et al.*,[60] this was because of the thermal decomposition of CYHPO with high temperature, which reduced the concentration of CYHPO and decreased the efficiency of the ODS process. At the reaction temperature of 393 K, it could be observed that the sulfur conversion rates dropped from 90.71% to 89.45%, and the reaction time was prolonged from 10 to 30 min (Fig. 10). The reason for this phenomenon was that MT-1 : 4 presented little adsorption capability for DBT and the desorption of DBT would occur as the reaction temperature increased. So, the sulfur content increased slightly in the model oil with the reaction time changed from 10 to 30 min, which were consistent with the results in Table 3. Since the complete conversion of DBT could be firstly achieved at 373 K within 15 min, 373 K was chosen as the optimal reaction temperature for the ODS system. The reaction time of this study was cut half at the same reaction temperature compared with the former report,[17] which investigated that the catalyst achieved a conversion rate of 99.90% within 30 min.

To investigate the ODS kinetics, the non-linear form was employed to attain the reaction rate constant of DBT.[7,61] The reaction rate was investigated by an empirical kinetic model (eqn (4)–(8)) without mass transfer limitations:

$$-\frac{d[C_{DBT}]}{dt} = k[C_{CYHPO}]^m[C_{DBT}]^n \quad (4)$$

The variation in CYHPO concentration was negligible compared with DBT concentration and the dosage of CYHPO was excessive (O/S molar ratio = 2). Hence, the CYHPO concentration was regarded as a constant. Therefore, the ODS reaction could be regarded as pseudo first order and the reaction rate was presented as

$$-\frac{d[C_{DBT}]}{dt} = k'[C_{DBT}]^n \quad (5)$$

and,

$$k' = k[C_{CYHPO}]^m \quad (6)$$

$$t = 0,\ C_{DBT} = C_{DBT,0} \text{ and } t = t,\ C_{DBT} = C_{DBT,t} \quad (7)$$

integrating eqn (5) yields:

$$\ln\left[\frac{C_{DBT,0}}{C_{DBT,t}}\right] = k't \quad (8)$$

where, the initial and instantaneous concentrations of sulfur were expressed as $C_{DBT,0}$ and $C_{DBT,t}$, respectively.

As presented in Fig. 11, the reaction time (t) and $\ln(C_{DBT,0}/C_{DBT,t})$ displayed a linear relationship for the ODS of DBT, demonstrating that pseudo first order kinetics fit well with the sulfur concentration in ODS reaction. The slopes of the straight lines were employed to gain the apparent rate constants (k') at different temperatures. Ultimately, the apparent activation energies were obtained by the Arrhenius equation $E_a = RT^2 \frac{d \ln k}{dT}$

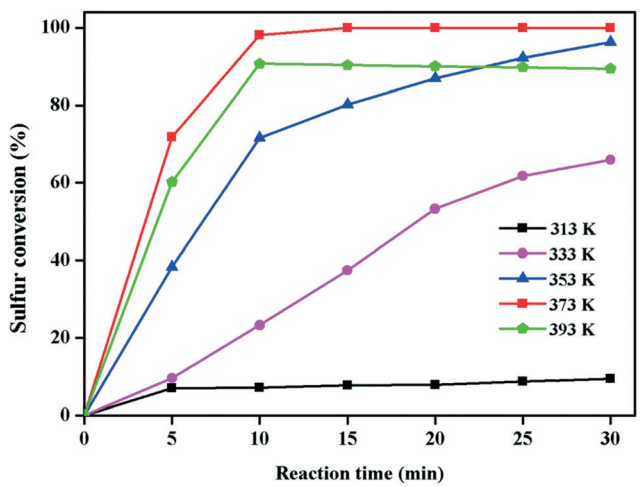

Fig. 10 Dependence of DBT conversion *vs.* reaction time on the ODS temperature over MT-1 : 4. Reaction conditions: 20 mL of model fuel, 0.10 g catalyst and O/S molar ratio of 2.

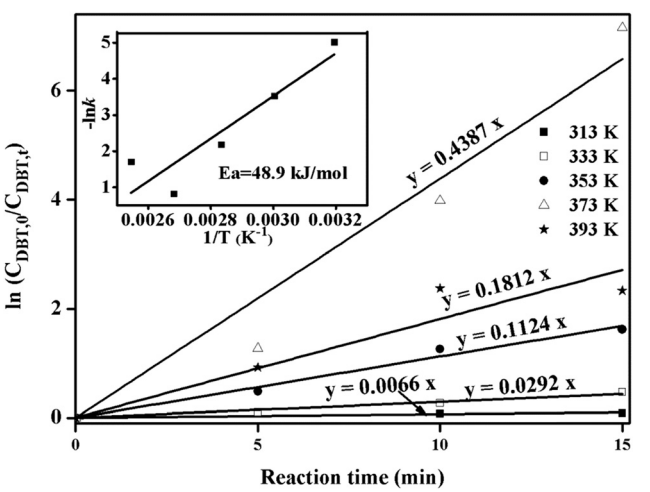

Fig. 11 Pseudo-first-order rate constants for the ODS reaction of DBT at 313 K, 333 K, 353 K, 373 K and 393 K over MT-1 : 4 (inset showed Arrhenius plot for DBT oxidation). Reaction conditions: 20 mL of model fuel, 0.10 g catalyst and O/S molar ratio of 2.

This journal is © The Royal Society of Chemistry 2019

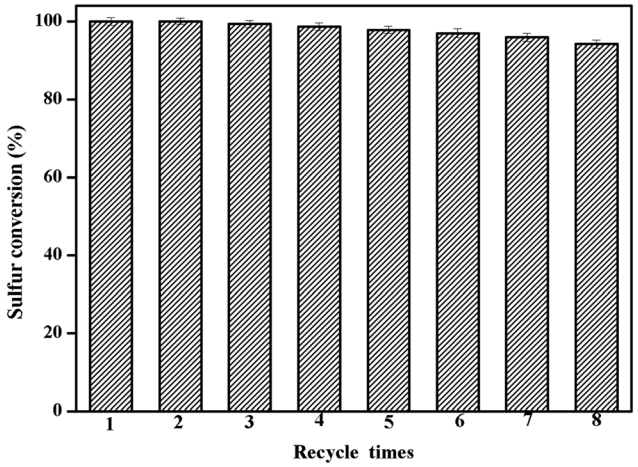

Fig. 12 Regeneration study of MT-1 : 4. Each regeneration step consisted of high temperature calcination of the catalyst at 823 K after the ODS reaction. Reaction conditions: O/S = 2.0, $V_{\text{model oil}}$ = 20 mL, M_{catalyst} = 0.10 g, t = 15 min, and T = 373 K.

and the result was 48.9 kJ mol^{-1} in the inset of Fig. 11, which was similar to the investigation of Bazyari *et al.*[36]

3.6. Evaluation of catalyst regenerability

There was no doubt that the regenerability of the catalysts is an extremely important factor in terms of industrial application. Therefore, in order to assess the regenerability of the MT-1 : 4, the repeated ODS experiments were performed. The used samples were regained by simple filtration, dried overnight at 333 K at the end of the reaction, and were then calcined at 823 K for 3 h. Finally, the obtained catalysts were reused in a new cycle. As seen in Fig. 12, there was no obvious decrease in the activity of the catalyst after 8 successive runs and the sulfur conversion rate still reached 94.56%, which indicated that MT-1 : 4 presented superior regenerability on the oxidative desulfurization of DBT. The above results suggested that MT-1 : 4 was a stable, recyclable, and cost-effective catalyst for industrial application.

3.7. ODS mechanism on MoO_3–TiO_2@MCM-22

Based on the above experimental data and characteristic analysis, it was concluded that MoO_3 and TiO_2 achieved the synergistic effect by regulating Lewis and Brønsted sites on the catalyst surface. In the coexistence of Mo and Ti, MT-1 : 4 contained the highest concentration of Brønsted and Lewis acid sites, and the highest CI value, which could promote the formation of peroxometallate complexes.[38] The probable mechanism for oxidative desulfurization with H_2O_2 involved the generation of peroxo-molybdate species and the following nucleophilic attack of the sulfur atoms in the sulfide on the peroxo species. Indeed, it was widely accepted that electrophilic oxidants oxidized DBT to sulfone.[62] Furthermore, sulfones as well as cyclohexanone were produced when DBT reacted with CYHPO and the products were detected by GC-MS in our previous researches.[9,17] Moreover, Mashio *et al.*[63] proposed that the coordination of *tert*-butyl hydroperoxide to Mo–O formed the five-member ring. Also, the polarization of the $Mo^{\delta+}$–$O^{\delta-}$ bond boosted the coordination of hydroperoxide to Mo–O when *tert*-butyl hydroperoxide was employed as the oxidant with a molybdenum catalyst.[64] Palomeque-Santiago *et al.*[20] suggested that the hydroperoxytungstate species could be formed by breaking the O–O peroxide bond when the tungsten oxide clusters have, at least, one exposed oxygen. Besides, Chen *et al.*[51] proposed that the main reactive species were hydroxyl radicals and electrons for ODS mechanism. Based on the above researches, the possible ODS mechanism of DBT on MoO_3–TiO_2@MCM-22 with CYHPO was deduced and is presented in Scheme 1. Firstly, a coordinated five-membered ring and a coordinated six-membered ring were formed respectively by the chemisorption of CYHPO on Mo–O and Ti–O active sites. In step 1 (Scheme 1), electron transfer would easily occur from Mo to neighboring O_2 atom and from Ti to neighboring O_4 atom due to the high electron density on Mo atoms and Ti atoms on the surface of MCM-22 (some electrons transferred from MCM-22 based on the XPS results), according to the studies.[32,51] This was inconsistent with the research of Julio González *et al.*,[65] which was most likely caused by a different reaction system. High electron density on O_2 and O_4 atoms made the O–O bond break much more easily and this caused the formation of ˙OH and ˙O radicals. In step 2 (Scheme 1), the formed ˙OH and ˙O radicals showed high oxidizability. One possibility was that the specific O_1 or O_3 atoms were nucleophilically attacked by the sulfur atoms of DBT, which resulted in the formation of sulfoxide and were further oxidized to sulfone. The other was that the sulfur atoms of DBT nucleophilically attacked the specific O_1 and O_3 atoms simultaneously,

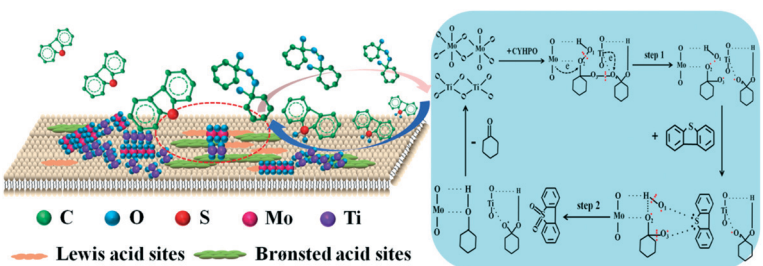

Scheme 1 The probable ODS mechanism of CYHPO on the MoO_3–TiO_2@MCM-22 catalyst.

causing the direct formation of sulfone, and Ti atoms broke the O–O bond at O_3–O_4 more easily than the Mo atoms due to the higher density of Ti atoms in the catalyst MT-1 : 4, which completely converted DBT to sulfone within 15 min. Thus, step 1 included electron transfer and O–O bond cleavage, step 2 was that specific O atoms were nucleophilically attacked by the sulfur atoms of DBT, both of which could act as the rate-limiting step.

4. Conclusions

In summary, a type of heterogeneous MoO_3–TiO_2@MCM-22 catalyst was successfully synthesized with high ODS performance. Characterizations by SEM, HRTEM, N_2 adsorption–desorption, XRD, FT-IR, XPS, and Py-FTIR showed that MoO_3 and TiO_2 were successfully supported on MCM-22. The catalyst MT-1 : 4 exhibited the highest ODS activity, which reached a sulfur conversion of 99.96% at 373 K, catalyst dosage of 0.10 g, and O/S molar ratio of 2.0 within 15 min. Importantly, the enhanced catalytic activity mainly resulted from the synergistic effect between MoO_3 and TiO_2, which was achieved by adjusting the concentration of Lewis and Brønsted acid sites on the surface of MCM-22. Besides, the kinetic studies revealed that ODS was a pseudo first-order kinetic process with an apparent activation energy of 48.9 kJ mol^{-1}. The possible ODS mechanism on MoO_3–TiO_2@MCM-22 included two steps, both of which could be rate-limiting. The former included electron transfer and O–O bond cleavage, and the latter was that the specific O atoms were nucleophilically attacked by the sulfur atoms of DBT. Moreover, the results of periodic and repeated ODS experiments suggested that MT-1 : 4 was a stable and recyclable catalyst. MoO_3–TiO_2@MCM-22 was a cost-effective material with ultra-deep performance for catalytic oxidative desulfurization of DBT and thus had superior potential for industrial application.

Conflicts of interest

There are no conflicts to declare.

Acknowledgements

This work was supported by the National Natural Science Foundation of China (Grant No.: 51978178, 51478172 and 51521006), the Department of Science and Technology of Guangdong Province of China (Contract No.: 2018S0011), the International S&T Cooperation Program of China (Contract No.: 2015DFG92750), the Natural Science Foundation of Zhejiang Province of China (Grant No.: LY17E080002), and the Department of Science and Technology of Hunan Province of China (Contract No.: 2017JJ2029 and 2017SK2362).

References

1 S. Subhan, A. U. Rahman, M. Yaseen, H. U. Rashid, M. Ishaq, M. Sahibzada and Z. F. Tong, *Fuel*, 2019, **237**, 793–805.
2 M. Zuo, X. Huang, J. Li, Q. Chang, Y. Duan, L. Yan, Z. Xiao, S. Mei, S. Lu and Y. Yao, *Catal. Sci. Technol.*, 2019, **9**, 2923–2930.
3 Q. Zhang, J. Zhang, H. Yang, Y. Dong, Y. Liu, L. Yang, D. Wei, W. Wang, L. Bai and H. Chen, *Catal. Sci. Technol.*, 2019, **9**, 2915–2922.
4 X. Zhang, Y. Shi and G. Liu, *Catal. Sci. Technol.*, 2016, **6**, 1016–1024.
5 K. Leng, X. Li, G. Ye, Y. Du, Y. Sun and W. Xu, *Catal. Sci. Technol.*, 2016, **6**, 7615–7622.
6 B. N. Bhadra, J. Y. Song, N. A. Khan and S. H. Jhung, *ACS Appl. Mater. Interfaces*, 2017, **9**, 31192–31202.
7 S. N. Wei, H. J. He, Y. Cheng, C. P. Yang, G. M. Zeng and L. Qiu, *RSC Adv.*, 2016, **6**, 103253–103269.
8 R. Yahya, M. Craven, E. F. Kozhevnikova, A. Steiner, P. Samunual, I. V. Kozhevnikov and D. E. Bergbreiter, *Catal. Sci. Technol.*, 2015, **5**, 818–821.
9 Z. Y. Long, C. P. Yang, G. M. Zeng, L. Y. Peng, C. H. Dai and H. J. He, *Fuel*, 2014, **130**, 19–24.
10 S. Wu, H. Li, X. Li, H. He and C. Yang, *Chem. Eng. J.*, 2018, **353**, 533–541.
11 S. Z. Wang and J. L. Wang, *Sci. Total Environ.*, 2019, **658**, 1367–1374.
12 S. B. Cao, R. Du, Y. Z. Peng, B. K. Li and S. Y. Wang, *Chem. Eng. J.*, 2019, **362**, 107–115.
13 S. Ribeiro, C. M. Granadeiro, P. Silva, F. A. Almeida Paz, F. F. de Biani, L. Cunha-Silva and S. S. Balula, *Catal. Sci. Technol.*, 2013, **3**, 2404–2414.
14 H. R. Zhang, Q. Zhang, L. Zhang, T. T. Pei, L. Dong, P. Y. Zhou, C. Q. Li and L. X. Xia, *Chem. Eng. J.*, 2018, **334**, 285–295.
15 S. W. Li, R. M. Gao, W. Zhang, Y. Zhang and J. S. Zhao, *Fuel*, 2018, **221**, 1–11.
16 S. X. Lu, H. Zhong, D. M. Mo, Z. Hu, H. L. Zhou and Y. Yao, *Green Chem.*, 2017, **19**, 1371–1377.
17 L. Kang, H. Y. Liu, H. J. He and C. P. Yang, *Fuel*, 2018, **234**, 1229–1237.
18 C. M. Granadeiro, L. S. Nogueira, D. Julião, F. Mirante, D. Ananias, S. S. Balula and L. Cunha-Silva, *Catal. Sci. Technol.*, 2016, **6**, 1515–1522.
19 B. Y. Zhang, Z. X. Jiang, J. Li, Y. N. Zhang, F. Lin, Y. Liu and C. Li, *J. Catal.*, 2012, **287**, 5–12.
20 J. F. Palomeque-Santiago, R. López-Medina, R. Oviedo-Roa, J. Navarrete-Bolaños, R. Mora-Vallejo and J. M. Martínez-Magadán, *Appl. Catal., B*, 2018, **236**, 326–337.
21 S. Wu, Y. Lin, C. Yang, C. Du, Q. Teng, Y. Ma, D. Zhang, L. Nie and Y. Zhong, *Chemosphere*, 2019, **237**, 124478.
22 S. Wu, H. He, X. Li, C. Yang, G. Zeng, B. Wu, S. He and L. Lu, *Chem. Eng. J.*, 2018, **341**, 126–136.
23 X. M. Yan, P. Mei, L. Xiong, L. Gao, Q. Yang and L. Gong, *Catal. Sci. Technol.*, 2013, **3**, 1985–1992.
24 X. L. Ren, G. Miao, Z. Y. Xiao, F. Y. Ye, Z. Li, H. H. Wang and J. Xiao, *Fuel*, 2016, **174**, 118–125.
25 A. T. Shah, B. Li and Z. E. A. Abdalla, *J. Colloid Interface Sci.*, 2009, **336**, 707–711.
26 S. F. Cheng, Y. M. Liu, J. B. Gao, L. L. Wang, X. L. Liu, G. H. Gao, P. Wu and M. Y. He, *Chin. J. Catal.*, 2006, **27**, 547–549.

 This journal is © The Royal Society of Chemistry 2019

27 K. Y. Leng, Y. Y. Sun, X. Zhang, M. Yu and W. Xu, *Fuel*, 2016, **174**, 9–16.
28 Y. Wang, T. Yokoi, S. Namba, J. N. Kondo and T. Tatsumi, *J. Catal.*, 2016, **333**, 17–28.
29 L. Qiu, Y. Cheng, C. P. Yang, G. M. Zeng, Z. Y. Long, S. N. Wei, K. Zhao and L. Luo, *RSC Adv.*, 2016, **6**, 17036–17045.
30 S. Lee and D. Kim, *Chem. Eng. J.*, 2019, **363**, 43–48.
31 M. Muñoz, M. A. Gallo, A. Gutiérrez-Alejandre, D. Gazzoli and C. I. Cabello, *Appl. Catal., B*, 2017, **219**, 683–692.
32 F. Li, L. J. France, Z. Cai, Y. Li, S. Liu, H. Lou, J. Long and X. Li, *Appl. Catal., B*, 2017, **214**, 67–77.
33 K. O. Christe, D. A. Dixon, D. McLemore, W. W. Wilson, J. A. Sheehy and J. A. Boatz, *J. Fluorine Chem.*, 2000, **101**, 151–153.
34 M. Cargnello, T. R. Gordon and C. B. Murray, *Chem. Rev.*, 2014, **114**, 9319–9345.
35 L. Liu and X. Chen, *Chem. Rev.*, 2014, **114**, 9890–9918.
36 A. Bazyari, A. A. Khodadadi, A. Haghighat Mamaghani, J. Beheshtian, L. T. Thompson and Y. Mortazavi, *Appl. Catal., B*, 2016, **180**, 65–77.
37 Z. F. Liu, J. Tabora and R. J. Davis, *J. Catal.*, 1994, **149**, 117–126.
38 G. Rodriguez-Gattorno, A. Galano and E. Torres-García, *Appl. Catal., B*, 2009, **92**, 1–8.
39 X. T. Ma, D. Zhou, X. Chu, D. Li, J. Wang, W. C. Song and Q. H. Xia, *Microporous Mesoporous Mater.*, 2017, **237**, 180–188.
40 D. Yue, J. S. Lei, Y. Peng, J. S. Li and X. D. Du, *Fuel*, 2018, **226**, 148–155.
41 J. Zhang, J. B. Li, R. W. Thring, X. Hu and X. Y. Song, *J. Hazard. Mater.*, 2012, **203–204**, 195–203.
42 Z. Wu, X. Yuan, H. Zhong, H. Wang, L. Jiang, G. Zeng, H. Wang, Z. Liu and Y. Li, *J. Mol. Liq.*, 2017, **247**, 215–229.
43 W. J. Wang, P. Xu, M. Chen, G. M. Zeng, C. Zhang, C. Zhou, Y. Yang, D. Huang, C. Lai, M. Cheng, L. Hu, W. Xiong, H. Guo and M. Zhou, *ACS Sustainable Chem. Eng.*, 2018, **6**, 15503–15516.
44 R. G. R. Avendaño, J. A. D. L. Reyes, T. Viveros and J. A. M. D. L. Fuente, *Catal. Today*, 2009, **148**, 12–18.
45 Y. Lin, S. H. Wu, X. Li, X. Wu, C. P. Yang, G. M. Zeng, Y. R. Peng, Q. Zhou and L. Lu, *Appl. Catal., B*, 2018, **227**, 557–570.
46 Y. Liu, X. Ma, S. Wang and J. Gong, *Appl. Catal., B*, 2007, **77**, 125–134.
47 C. P. Yang, H. Qian, X. Li, Y. Cheng, H. J. He, G. M. Zeng and J. Y. Xi, *Trends Biotechnol.*, 2018, **36**, 673–685.
48 Y. Zhang and S. J. Park, *Appl. Catal., B*, 2019, **240**, 92–101.
49 H. Liu, Y. P. Li, C. L. Yin, Y. L. Wu, Y. M. Chai, D. M. Dong, X. H. Li and C. G. Liu, *Appl. Catal., B*, 2016, **198**, 493–507.
50 Q. Li, H. J. Su and T. W. Tan, *Biochem. Eng. J.*, 2008, **38**, 212–218.
51 K. Chen, X. M. Zhang, X. F. Yang, M. G. Jiao, Z. Zhou, M. H. Zhang, D. H. Wang and X. H. Bu, *Appl. Catal., B*, 2018, **238**, 263–273.
52 Y. Lin, X. Wu, Y. Han, C. P. Yang, Y. Ma, C. Du, Q. Teng, H. Y. Liu and Y. Y. Zhong, *Appl. Catal., B*, 2019, **258**, 117969.
53 R. J. Davis and Z. Liu, *Chem. Mater.*, 1997, **9**, 2311–2324.
54 V. V. Ordomsky, D. S. J. Van, J. C. Schouten and T. A. Nijhuis, *ChemSusChem*, 2012, **5**, 1812–1819.
55 T. C. Chou, *Pharmacol. Rev.*, 2006, **58**, 621–681.
56 Y. Zhang, G. Li, L. H. Kong and H. Lu, *Fuel*, 2018, **219**, 103–110.
57 Q. Zhou, Y. Lin, X. Li, C. P. Yang, Z. F. Han, G. M. Zeng, L. Lu and S. He, *Bioresour. Technol.*, 2018, **249**, 457–463.
58 Y. Lin, S. H. Wu, C. P. Yang, M. Chen and X. Li, *Appl. Catal., B*, 2019, **245**, 71–86.
59 B. Pawelec, R. M. Navarro, J. M. Campos-Martin and J. L. G. Fierro, *Catal. Sci. Technol.*, 2011, **1**, 23–42.
60 C. P. Yang, K. Zhao, Y. Cheng, G. M. Zeng, M. M. Zhang, J. J. Shao and L. Lu, *Sep. Purif. Technol.*, 2016, **163**, 153–161.
61 R. Zhuan and J. L. Wang, *Sci. Total Environ.*, 2019, **668**, 67–73.
62 A. E. S. Choi, S. Roces, N. Dugos and M. W. Wan, *Fuel*, 2016, **180**, 127–136.
63 F. Mashio and S. I. Kato, *Yuki Gosei Kagaku Kyokaishi*, 1968, **26**, 367–374.
64 D. Wang, E. W. Qian, H. Amano, K. Okata, A. Ishihara and T. Kabe, *Appl. Catal., A*, 2003, **253**, 91–99.
65 J. González, J. A. Wang, L. Chen, M. Manríquez, J. Salmones, R. Limas and U. Arellano, *J. Solid State Chem.*, 2018, **263**, 100–114.